Chaos
An Interdisciplinary Journal of Nonlinear Science

RESEARCH ARTICLE | DECEMBER 12 2023

Low-dimensional behavior of a Kuramoto model with inertia and Hebbian learning

Tachin Ruangkriengsin ; Mason A. Porter

Chaos 33, 123122 (2023)
https://doi.org/10.1063/5.0092378

Low-dimensional behavior of a Kuramoto model with inertia and Hebbian learning

Cite as: Chaos 33, 123122 (2023); doi: 10.1063/5.0092378
Submitted: 22 March 2022 · Accepted: 3 August 2023 ·
Published Online: 12 December 2023

Tachin Ruangkriengsin[1] and Mason A. Porter[1,2,a)]

AFFILIATIONS

[1]Department of Mathematics, University of California Los Angeles, Los Angeles, California 90095, USA
[2]Santa Fe Institute, Santa Fe, New Mexico 87501, USA

[a)]**Author to whom correspondence should be addressed:** mason@math.ucla.edu

ABSTRACT

We study low-dimensional dynamics in a Kuramoto model with inertia and Hebbian learning. In this model, the coupling strength between oscillators depends on the phase differences between the oscillators and changes according to a Hebbian learning rule. We analyze the special case of two coupled oscillators, which yields a five-dimensional dynamical system that decouples into a two-dimensional longitudinal system and a three-dimensional transverse system. We readily write an exact solution of the longitudinal system, and we then focus our attention on the transverse system. We classify the stability of the transverse system's equilibrium points using linear stability analysis. We show that the transverse system is dissipative and that all of its trajectories are eventually confined to a bounded region. We compute Lyapunov exponents to infer the transverse system's possible limiting behaviors, and we demarcate the parameter regions of three qualitatively different behaviors. Using insights from our analysis of the low-dimensional dynamics, we examine the original high-dimensional system in a situation in which we draw the intrinsic frequencies of the oscillators from Gaussian distributions with different variances.

Synchronization occurs ubiquitously in many systems,[1] such as in the electrical impulses of neurons and the flashing of fireflies. In response to changes in external environmental conditions, many systems of coupled oscillators adapt to enhance collective behavior. One example of adaptation is plasticity in networks of neurons, where the synaptic strengths between neurons change based on their relative spike times or on other features.[2] Another example of adaptation occurs in groups of fireflies,[3] which have been modeled using coupled phase oscillators with inertia. In situations like these two examples, adaptation can accelerate the synchronization of oscillators with similar phases while simultaneously facilitating global synchronization. In our work, we consider both plasticity and inertia by studying a modified version of the ubiquitous Kuramoto model of coupled oscillators.[4] To examine the interplay between oscillator plasticity and inertia, we mathematically analyze a small system of these coupled oscillators and use the results of this analysis to gain insights into larger systems of such oscillators.

I. INTRODUCTION

Researchers have analyzed systems of coupled oscillators to study collective behavior in many situations,[1] such as flashing in groups of fireflies,[5] the motion of pedestrians on the Millennium Bridge,[6,7] pacemaker conduction,[8] and singing in frogs.[9] In 1975, Yoshiki Kuramoto modeled a collection of coupled biological oscillators as a system of first-order differential equations in which each variable corresponds to the phase of an oscillator.[10] In this model, which is now known as the Kuramoto model, he assumed that the instrinsic frequency of each oscillator is chosen from a fixed probability distribution. He also assumed all-to-all coupling of these oscillators and that each oscillator i is influenced by each other oscillator j by an amount that is proportional to the sine of their phrase difference $\phi_j - \phi_i$.

One natural way to extend the original Kuramoto model is by incorporating a second-order term to include inertia.[11] This extension was employed as part of an adaptive model to explain the ability of the firefly *Pteroptyx malaccae* to synchronize its flashing.[3] Researchers have also employed Kuramoto models with inertia

to study disordered arrays of Josephson junctions,[12] decentralized power grids,[13] and a variety of other phenomena. Following the setup of Tanaka *et al.*,[14] we consider a Kuramoto model with inertia of the form

$$m_i \frac{d^2\phi_i}{dt^2} + \frac{d\phi_i}{dt} = \omega_i + \frac{1}{N}\sum_{j=1, j\neq i}^{N} K_{ij}\sin(\phi_j - \phi_i), \quad i \in \{1, 2, \ldots, N\}, \tag{1}$$

where $\phi_i \in [0, 2\pi)$ is the phase of the ith oscillator, ω_i is its intrinsic frequency, m_i is its mass, N is the number of oscillators, and $K_{ij} = K_{ji}$ is the symmetric coupling strength between the ith and jth oscillators.

In the original formulation of the Kuramoto model, the coupling strength K_{ij} is constant. However, this assumption is too restrictive for some problems. For example, in neuroscience, neurons exhibit synaptic plasticity when their strengths change in response to activity-dependent mechanisms.[2] According to Hebbian theory,[15] the synaptic strength between two neurons increases when they are active simultaneously. If we view regularly spiking neurons as coupled oscillators, the time-dependent coupling strength $K_{ij} = K_{ij}(t)$ increases when the phase difference between oscillators i and j decreases.

Adaptive Kuramoto models (without inertia) have been studied extensively in the past decade.[16–18] They have very interesting dynamics, such as rich bifurcation structures,[19] the coexistence of multiple distinct clusters of oscillators,[20] and "heterogeneous nucleation" (which involves both single-step and multi-step transitions to synchronization).[21] Kuramoto models with Hebbian learning have also been studied with multiplex[22] and polyadic[23] interactions between oscillators. Rigorous mean-field[24] and continuum[25] limits have been developed to study adaptive network dynamics in a broad class of Kuramoto models.

Researchers have proposed a variety of functions to model Hebbian changes in the coupling between oscillators[20,26–32] in Kuramoto models without inertia. We follow Niyogi and English[26] and suppose that the coupling strengths satisfy

$$\frac{dK_{ij}}{dt} = \beta(\alpha\cos(\phi_j - \phi_i) - K_{ij}), \tag{2}$$

where $\alpha > 0$ is the *learning enhancement factor* and $\beta > 0$ is the *learning rate*. Because $\cos(\phi_j - \phi_i) = \cos(\phi_i - \phi_j)$, we let $K_{ij}(0) = K_{ji}(0)$ so that $K_{ij}(t) = K_{ji}(t)$ for all $t \geq 0$ is the symmetric coupling strength between the ith and jth oscillators. Equations (1) and (2) constitute a dynamical system, with $N + \frac{(N-1)(N)}{2} = \frac{N(N+1)}{2}$ equations, of coupled Kuramoto oscillators with inertia and Hebbian learning. We refer to this dynamical system as our *Hebbian Kuramoto model*. We first consider the case $N = 2$ and study the resulting low-dimensional system. We then use insights from our analysis with $N = 2$ to briefly consider a higher-dimensional system (with $N = 50$).

Our paper proceeds as follows. In Sec. II, we analyze our Hebbian Kuramoto model with $N = 2$ oscillators. We consider both its transverse and longitudinal coordinates, which decouple. We obtain an exact solution of the longitudinal system and perform linear stability analysis of the equilibria of the transverse system. In Sec. III, we show that the transverse dynamical system is dissipative and contracting. In Sec. IV, we demarcate the different behaviors of the transverse system in a two-dimensional (2D) parameter space. We briefly examine our Hebbian Kuramoto model with $N = 50$ oscillators in Sec. V, and we conclude in Sec. VI.

II. LINEAR STABILITY ANALYSIS OF A SYSTEM OF $N = 2$ COUPLED OSCILLATORS

We examine our Hebbian Kuramoto model [see Eqs. (1) and (2)] with $N = 2$ oscillators with identical masses. This yields the five-dimensional (5D) dynamical system

$$m\frac{d^2\phi_1}{dt^2} + \frac{d\phi_1}{dt} = \omega_1 + \frac{1}{2}k\sin(\phi_2 - \phi_1), \tag{3}$$

$$m\frac{d^2\phi_2}{dt^2} + \frac{d\phi_2}{dt} = \omega_2 + \frac{1}{2}k\sin(\phi_1 - \phi_2), \tag{4}$$

$$\frac{dk}{dt} = \beta(\alpha\cos(\phi_2 - \phi_1) - k), \tag{5}$$

where $k := K_{12} = K_{21}$.

To analyze the dynamical system (3)–(5), we consider the transverse coordinate $\phi := \phi_1 - \phi_2$ and longitudinal coordinate $\psi := \phi_1 + \phi_2$. In prior studies of synchronization, it has been very insightful to analyze dynamical systems using such coordinates.[33,34] Taking the difference and sum of (3) and (4) yields

$$m\frac{d^2\phi}{dt^2} + \frac{d\phi}{dt} = \omega_1 - \omega_2 - k\sin(\phi), \tag{6}$$

$$m\frac{d^2\psi}{dt^2} + \frac{d\psi}{dt} = \omega_1 + \omega_2. \tag{7}$$

In these new coordinates, the 5D dynamical system (3)–(5) decouples into two independent systems: a three-dimensional (3D) dynamical system, which is given by Eqs. (5) and (6), in the transverse direction and a 2D dynamical system (7) in the longitudinal direction.

Equation (7) is a second-order ordinary differential equation with constant coefficients. Its solution is

$$\psi(t) = C_1 + (\omega_1 + \omega_2)t + C_2\, e^{-\frac{1}{m}t}, \tag{8}$$

where the initial values $\psi(0)$ and $\psi'(0)$ determine the integration constants C_1 and C_2. When $t \to \infty$, we see that $\frac{d\psi}{dt} \approx \omega_1 + \omega_2$ for any initial values. Therefore, the sum of the oscillators' phases eventually increases approximately linearly as a function of time.

The transverse dynamical system [see Eqs. (5) and (6)] does not have an exact solution. Therefore, we write it as a 3D dynamical system to analyze its behavior. We specify the domains of the phase difference $\phi \in [-\pi, \pi)$, the derivative $\gamma := \frac{d\phi}{dt} \in \mathbb{R}$ of the phase difference, and the intrinsic-frequency difference $\omega := \omega_1 - \omega_2 \in \mathbb{R}$. By symmetry, we assume without loss of generality that $\omega \geq 0$. We reduce the number of parameters in the transverse system by rescaling time and defining $\tilde{k} := k/\beta$, $\tilde{\alpha} = \alpha/\beta$, $\tilde{\omega} := \omega/\beta$, $\tilde{\gamma} := \gamma/\beta$, $\tilde{m} := \beta m$, and $\tilde{t} := \beta t$. These transformations indicate that we do not need the parameter β, so we take $\beta = 1$ without loss of generality and write

$$\frac{d\phi}{dt} = \gamma, \tag{9}$$

$$\frac{d\gamma}{dt} = \frac{1}{m}(-\gamma + \omega - k\sin(\phi)), \tag{10}$$

$$\frac{dk}{dt} = \alpha\cos(\phi) - k, \tag{11}$$

where we drop the tildes from our notation for convenience.

We obtain the equilibrium points (ϕ^*, γ^*, k^*) of the dynamical system (9)–(11) by setting $\frac{d\phi}{dt} = \frac{d\gamma}{dt} = \frac{dk}{dt} = 0$. This implies that $\gamma^* = -\gamma^* + \omega - k^*\sin(\phi^*) = 0$ and $\alpha\cos(\phi^*) - k^* = 0$. Simplifying yields

$$\sin(2\phi^*) = \frac{2\omega}{\alpha}, \tag{12}$$

so the equilibrium points exist if and only if $\alpha \geq 2\omega$. Because $\phi \in [-\pi, \pi)$, we obtain four equilibria: $P_1 = \left(\frac{1}{2}\arcsin\left(\frac{2\omega}{\alpha}\right), 0, \alpha\cos\left(\frac{1}{2}\arcsin\left(\frac{2\omega}{\alpha}\right)\right)\right)$, $P_2 = \left(\frac{\pi}{2} - \frac{1}{2}\arcsin\left(\frac{2\omega}{\alpha}\right), 0, \alpha\sin\left(\frac{1}{2}\arcsin\left(\frac{2\omega}{\alpha}\right)\right)\right)$, $P_3 = \left(-\pi + \frac{1}{2}\arcsin\left(\frac{2\omega}{\alpha}\right), 0, -\alpha\cos\left(\frac{1}{2}\arcsin\left(\frac{2\omega}{\alpha}\right)\right)\right)$, and $P_4 = \left(-\frac{\pi}{2} - \frac{1}{2}\arcsin\left(\frac{2\omega}{\alpha}\right), 0, -\alpha\sin\left(\frac{1}{2}\arcsin\left(\frac{2\omega}{\alpha}\right)\right)\right)$.

The Jacobian matrix of the linearization of (9)–(11) at the equilibrium points is

$$J(\phi^*, \gamma^*, k^*) = \begin{bmatrix} 0 & 1 & 0 \\ -\frac{k^*}{m}\cos(\phi^*) & -\frac{1}{m} & -\frac{\sin(\phi^*)}{m} \\ -\alpha\sin(\phi^*) & 0 & -1 \end{bmatrix} = \begin{bmatrix} 0 & 1 & 0 \\ -\frac{\alpha\cos^2(\phi^*)}{m} & -\frac{1}{m} & -\frac{\sin(\phi^*)}{m} \\ -\alpha\sin(\phi^*) & 0 & -1 \end{bmatrix}. \tag{13}$$

The eigenvalues λ of $J(\phi^*, \gamma^*, k^*)$ satisfy

$$-\lambda(\lambda+1)\left(\lambda + \frac{1}{m}\right) - \frac{\alpha\cos^2(\phi^*)}{m}(\lambda+1) + \frac{\alpha\sin^2(\phi^*)}{m} = 0. \tag{14}$$

Using (12), we simplify Eq. (14) for each equilibrium point. The equilibrium points P_1 and P_3 both give

$$-2\lambda(\lambda+1)(m\lambda+1) - \left(\alpha + \sqrt{\alpha^2 - 4\omega^2}\right)(\lambda+1) + \left(\alpha - \sqrt{\alpha^2 - 4\omega^2}\right) = 0. \tag{15}$$

The equilibrium points P_2 and P_4 both give

$$-2\lambda(\lambda+1)(m\lambda+1) - \left(\alpha - \sqrt{\alpha^2 - 4\omega^2}\right)(\lambda+1) + \left(\alpha + \sqrt{\alpha^2 - 4\omega^2}\right) = 0. \tag{16}$$

When $\alpha = 2\omega$, we obtain $P_1 = P_2$ and $P_3 = P_4$. These mergers of equilibrium points are saddle–node bifurcations that arise from the same characteristic equation,

$$\lambda(\lambda+1)(m\lambda+1) + \frac{\alpha\lambda}{2} = \lambda\left(m\lambda^2 + (m+1)\lambda + 1 + \frac{\alpha}{2}\right) = 0, \tag{17}$$

which gives $\lambda = 0$ and $\lambda = \frac{-(m+1)\pm\sqrt{(m-1)^2 - 2m\alpha}}{2m}$.

When $\alpha > 2\omega$, we have the following proposition.

Proposition 1. *Consider the dynamical system (9)–(11) with $\alpha > 2\omega$. Let $u := \alpha + \sqrt{\alpha^2 - 4\omega^2}$ and $v := \alpha - \sqrt{\alpha^2 - 4\omega^2}$. The following statements hold:*

1. *Let Γ_1 be the region in the (u, v) plane with $0 \leq v \leq u \leq \frac{2(m^2-m+1)}{3m}$ that is bounded by the curves*

$$v = u - \frac{\left(m+1+\sqrt{4(m+1)^2 - 6m(u+2)}\right)\left(\sqrt{4(m+1)^2 - 6m(u+2)} - 2(m+1)\right)^2}{54m^2},$$

$$v = u - \frac{\left(m+1-\sqrt{4(m+1)^2 - 6m(u+2)}\right)\left(\sqrt{4(m+1)^2 - 6m(u+2)} + 2(m+1)\right)^2}{54m^2}.$$

   If $(u, v) \notin \Gamma_1$, then the Jacobian matrix at the equilibria P_1 and P_3 has a negative real eigenvalue and two complex-conjugate eigenvalues with a negative real part. Otherwise, the Jacobian matrix at the equilibria P_1 and P_3 has three negative real eigenvalues.

2. *Let Γ_2 be the region in the (u, v) plane with $0 \leq v \leq u$ and $v \leq \frac{2(m^2-m+1)}{3m}$ that is bounded by the curves*

$$u = v - \frac{\left(m+1+\sqrt{4(m+1)^2 - 6m(v+2)}\right)\left(\sqrt{4(m+1)^2 - 6m(v+2)} - 2(m+1)\right)^2}{54m^2},$$

$$u = v - \frac{\left(m+1-\sqrt{4(m+1)^2 - 6m(v+2)}\right)\left(\sqrt{4(m+1)^2 - 6m(v+2)} + 2(m+1)\right)^2}{54m^2}.$$

   If $(u, v) \notin \Gamma_2$, the Jacobian matrix at the equilibria P_2 and P_4 has a positive real eigenvalue and two complex-conjugate eigenvalues with a negative real part. Otherwise, the Jacobian matrix at the equilibria P_2 and P_4 has one positive real eigenvalue and two negative real eigenvalues.

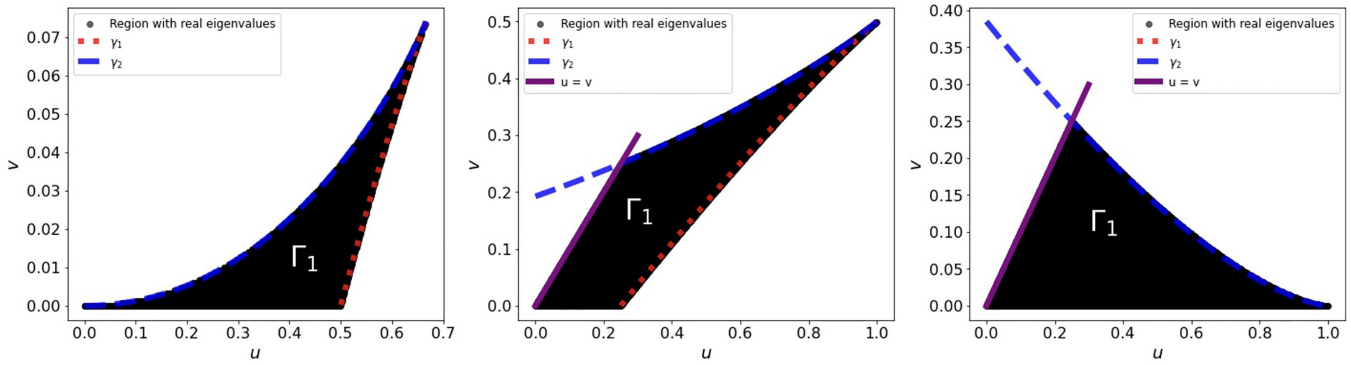

FIG. 1. The region Γ_1 in the (u, v) plane with (left) $m = 1$, (center) $m = 2$, and (right) $m = 0.5$. In this region, the Jacobian matrix at the equilibria P_1 and P_3 has negative real eigenvalues. We use γ_1 to denote the curve $u = v - \frac{\left(m+1+\sqrt{4(m+1)^2-6m(v+2)}\right)\left(\sqrt{4(m+1)^2-6m(v+2)}-2(m+1)\right)^2}{54m^2}$ and γ_2 to denote the curve $u = v - \frac{\left(m+1-\sqrt{4(m+1)^2-6m(v+2)}\right)\left(\sqrt{4(m+1)^2-6m(v+2)}+2(m+1)\right)^2}{54m^2}$.

We prove Proposition 1 in the Appendix. Additionally, we empirically verify Proposition 1 by performing numerical computations on a uniform grid in the (u, v) plane. We construct a region Γ_1 in the (u, v) plane for which the Jacobian matrix at the equilibria P_1 and P_3 has three real eigenvalues. We let $(u, v) \in \left[0, \frac{2(m^2-m+1}{3m}\right] \times \left[0, \frac{2(m^2-m+1)}{3m}\right]$, divide this rectangle into a uniform grid with 1000×1000 points, and calculate the eigenvalues of the Jacobian matrix at the equilibria P_1 and P_3 at each grid point. In Fig. 1, we plot the region Γ_1 and its boundary. The boundary of the region Γ_1 matches well with the boundary of the region that we obtain with numerical simulations. The same is true for the region Γ_2.

III. DISSIPATION AND CONTRACTION IN THE DYNAMICAL SYSTEM (9)–(11)

A dynamical system $\frac{d\vec{x}}{dt} = f(\vec{x})$ is dissipative if the volume of any fixed region of phase space contracts as a function of time. For a constant divergence $\nabla \cdot f < 0$, the volume contracts exponentially fast with rate $\nabla \cdot f$. Calculating the divergence $\nabla \cdot f$ that is associated with equations (9)–(11) gives

$$\frac{\partial}{\partial\phi}(\gamma) + \frac{1}{m}\frac{\partial}{\partial\gamma}(-\gamma + \omega - k\sin\phi) + \frac{\partial}{\partial k}(\alpha\cos\phi - k) = -\frac{1}{m} - 1 < 0.$$

Therefore, our low-dimensional transverse system is dissipative, with a volume contraction rate of $-\frac{1}{m} - 1$. We also show that all trajectories of (9)–(11) are eventually confined to a bounded region of phase space.

Theorem 1. *Suppose that $(\phi(t), \gamma(t), k(t))_{t\geq 0}$ is a trajectory of the dynamical system (9)–(11), and let $(\phi(0), \gamma(0), k(0)) = (\phi_0, \gamma_0, k_0)$ denote its initial condition. For all $\epsilon > 0$, there exists some time $T_\epsilon \geq 0$ such that $|k(t)| \leq \alpha + \epsilon$ and $|\gamma| \leq \omega + \alpha + \epsilon$ for all times $t \geq T_\epsilon$.*

Proof. We start by multiplying both sides of (11) by the integrating factor e^t to obtain

$$\frac{d}{dt}\left(k(t)\,e^t\right) = \alpha\cos\phi(t)\,e^t$$
$$\implies k(t)\,e^t - k(0) = \int_0^t \alpha\cos\phi(\tilde{t})\,e^{\tilde{t}}\,d\tilde{t}$$
$$\implies |k(t)\,e^t - k_0| \leq \int_0^t \alpha|\cos\phi(\tilde{t})|e^{\tilde{t}}\,d\tilde{t} \leq \int_0^t \alpha\,e^{\tilde{t}}\,d\tilde{t} = \alpha\left(e^t - 1\right).$$

Consequently, we see that $|k(t)| \leq \alpha + \frac{|k_0|-\alpha}{e^t} \leq \alpha + \epsilon$ for all times $t \geq T_1 = \ln\left(\left|\frac{|k_0|-\alpha}{\epsilon}\right| + 1\right)$. Similarly, we multiply both sides of (10) by the integrating factor $e^{t/m}$ to obtain

$$\frac{d}{dt}(\gamma\,e^{t/m}) = \frac{\omega\,e^{t/m}}{m} - \frac{k(t)\,e^{t/m}\sin\phi(t)}{m}$$
$$\implies \gamma(t)\,e^{t/m} - \gamma_0 = \int_0^t \left[\frac{\omega\,e^{\tilde{t}/m}}{m} - \frac{k(\tilde{t})\,e^{\tilde{t}/m}\sin\phi(\tilde{t})}{m}\right] d\tilde{t}.$$

Let $T_2 \in \mathbb{R}$ such that $|k(t)| \leq \alpha + \frac{\epsilon}{2}$ for all $t \geq T_2$. For all $t \geq T_2$, we then have

$$\left|\gamma(t)\,e^{\frac{t}{m}} - \gamma_0\right| \leq \int_0^t \left|\frac{\omega\,e^{\tilde{t}/m}}{m} - \frac{k(\tilde{t})\,e^{\tilde{t}/m}\sin\phi(\tilde{t})}{m}\right| d\tilde{t} \leq \int_0^t \frac{\omega\,e^{\tilde{t}/m}}{m}\,d\tilde{t} + \int_0^t \frac{|k(\tilde{t})\,e^{\tilde{t}/m}|}{m}\,d\tilde{t}$$

$$
\begin{aligned}
&\le \omega(e^{t/m}-1)+\int_0^{T_2}\frac{|k(\tilde{t})\,e^{\tilde{t}/m}|}{m}\,d\tilde{t}\\
&\quad+\int_{T_2}^{t}\frac{(\alpha+\frac{\epsilon}{2})\,e^{\tilde{t}/m}}{m}\,d\tilde{t}\\
&=\omega(e^{t/m}-1)+\int_0^{T_2}\frac{|k(\tilde{t})\,e^{\tilde{t}/m}|}{m}\,d\tilde{t}\\
&\quad+\left(\alpha+\frac{\epsilon}{2}\right)(e^{t/m}-e^{T_2/m})\\
&=\left(\omega+\alpha+\frac{\epsilon}{2}\right)e^{t/m}-\omega-\left(\alpha+\frac{\epsilon}{2}\right)e^{T_2/m}\\
&\quad+\int_0^{T_2}\frac{|k(\tilde{t})\,e^{\tilde{t}/m}|}{m}\,d\tilde{t}.
\end{aligned}
$$

Consequently,

$$
|\gamma(t)|\le\left(w+\alpha+\frac{\epsilon}{2}\right)+\frac{\left|-\omega-\left(\alpha+\frac{\epsilon}{2}\right)e^{T_2/m}+\int_0^{T_2}\frac{|k(\tilde{t})\,e^{\tilde{t}/m}|}{m}\,d\tilde{t}+|\gamma_0|\right|}{e^{t/m}}.
$$

The numerator of the second term is constant, so

$$
\lim_{t\to\infty}\frac{\left|-\omega-\left(\alpha+\frac{\epsilon}{2}\right)e^{T_2/m}+\int_0^{T_2}\frac{|k(\tilde{t})\,e^{\tilde{t}/m}|}{m}\,d\tilde{t}+|\gamma_0|\right|}{e^{t/m}}=0.
$$

Therefore, there exists a constant $T_3\in\mathbb{R}$ such that

$$
\frac{\left|-\omega-\left(\alpha+\frac{\epsilon}{2}\right)e^{T_2/m}+\int_0^{T_2}\frac{|k(\tilde{t})\,e^{\tilde{t}/m}|}{m}\,d\tilde{t}+|\gamma_0|\right|}{e^{t/m}}\le\frac{\epsilon}{2}
$$

for all $t\ge T_3$. We conclude that $k(t)\le\alpha+\epsilon$ and $\gamma(t)\le\omega+\alpha+\epsilon$ for all $t\ge T_\epsilon=\max\{T_1,T_2,T_3\}$, as desired. □

We have just shown that the dynamical system (9)–(11) is dissipative and that all of its trajectories are eventually confined to a bounded region. To obtain further insight into the possible limiting behaviors of the dynamical system (9)–(11), we compute its Lyapunov exponents near the origin with a numerical approach[35] that is based on the algorithms in Ref. 36. We show these Lyapunov exponents in Figs. 2 and 3.

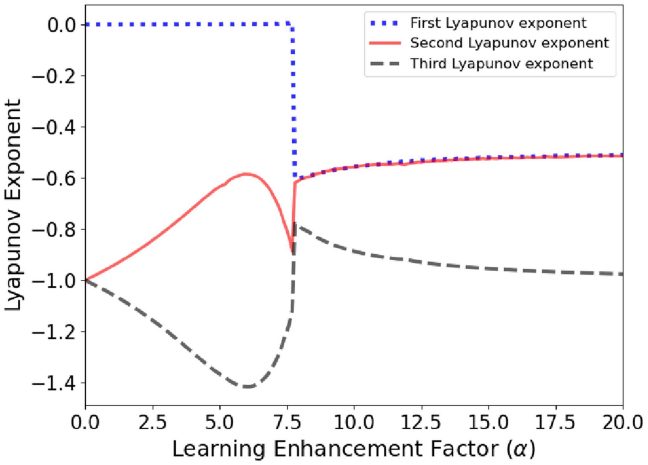

FIG. 2. Lyapunov exponents for trajectories near the origin $(0,0,0)$ for the dynamical system (9)–(11) with mass $m=1$, intrinsic-frequency difference $\omega=3$, and different values of the learning enhancement factor α.

In our computations, we obtain either three negative Lyapunov exponents or one 0 Lyapunov exponent and two negative Lyapunov exponents. A chaotic attractor requires one positive Lyapunov exponent, and a quasiperiodic orbit on a 2-torus requires two 0 Lyapunov exponents.[37] Therefore, the attractors of the dynamical system (9)–(11) must consist of equilibrium points, periodic orbits, or unions of periodic orbits and equilibrium points. When we increase the learning enhancement factor α for fixed mass $m=1$ and fixed intrinsic-frequency difference $\omega=3$, we move from a region with two negative Lyapunov exponents to a region with three negative Lyapunov exponents. To examine how the transition from two negative Lyapunov exponents to three negative Lyapunov exponents depends on other parameters, we compute the largest

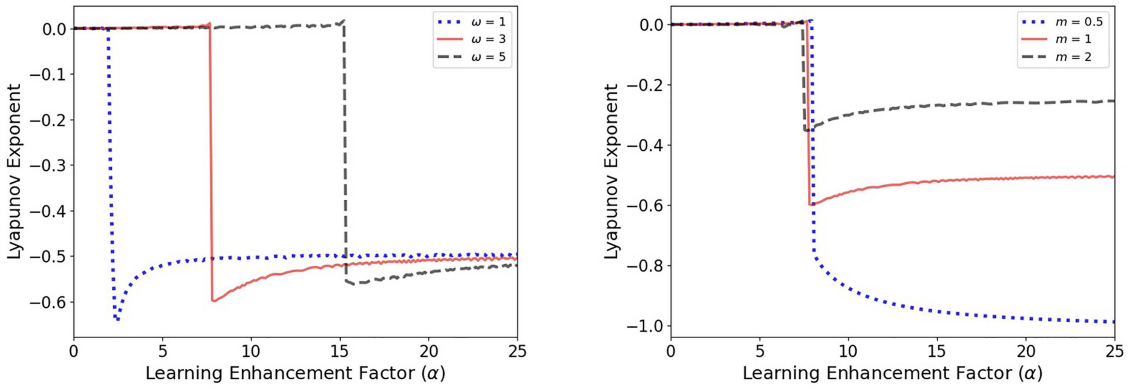

FIG. 3. Largest Lyapunov exponent for trajectories near the origin $(0,0,0)$ for the dynamical system (9)–(11). (Left) We fix the mass to $m=1$ and consider intrinsic-frequency differences of $\omega=0.1$, $\omega=0.3$, and $\omega=1$. (Right) We fix the intrinsic-frequency difference to $\omega=1$ and consider masses of $m=0.5$, $m=1$, and $m=2$.

Lyapunov exponents for several values of m and ω (see Fig. 3). For larger values of ω, the transition occurs at larger values of α, whereas the mass m mostly affects only the magnitude of the largest Lyapunov exponent.

To further examine contraction in the dynamical system (9)–(11), we define the energy function

$$E(\phi,\gamma,k) := \frac{\alpha m\gamma^2}{2} - \alpha\omega\phi - \alpha k\cos\phi + \frac{k^2}{2}. \tag{18}$$

Consider the critical points of E. At these points,

$$\frac{\partial E}{\partial \phi} = 0 \Longrightarrow -\alpha\omega + \alpha k\sin\phi = 0,$$
$$\frac{\partial E}{\partial \gamma} = 0 \Longrightarrow \alpha m\gamma = 0,$$
$$\frac{\partial E}{\partial k} = 0 \Longrightarrow -\alpha\cos\phi + k = 0.$$

These three equations are the same equations for the equilibrium points of the dynamical system (9)–(11). Therefore, the equilibrium points are the critical points of E. In the interior of the domain $(\phi,\gamma,k) \in [-\pi,\pi)\times\mathbb{R}\times\mathbb{R}$, we calculate

$$\begin{aligned}\frac{d}{dt}E(\phi,\gamma,k) &= \alpha m\gamma\frac{d\gamma}{dt} - \alpha\omega\frac{d\phi}{dt}\\ &\quad - \alpha\left(-k\sin\phi\frac{d\phi}{dt} + \cos\phi\frac{dk}{dt}\right) + k\frac{dk}{dt}\\ &= \alpha m\gamma\frac{d\gamma}{dt} + (\alpha k\sin\phi - \alpha\omega)\frac{d\phi}{dt} + (k - \alpha\cos\phi)\frac{dk}{dt}\\ &= \alpha\gamma(-\gamma + \omega - k\sin\phi) + (\alpha k\sin\phi - \alpha\omega)\gamma\\ &\quad - (k - \alpha\cos\phi)^2\\ &= -(\alpha\gamma^2 + (k - \alpha\cos\phi)^2) \le 0.\end{aligned}$$

Therefore, the energy of a trajectory of the dynamical system (9)–(11) never increases with time and that the time derivative of the energy is independent of m. The energy E is a Lyapunov functional in the interior of the region $\{(\phi,\gamma,k)|(\phi,\gamma,k)\in[-\pi,\pi)\times\mathbb{R}\times\mathbb{R}\}$. Because of the term $\alpha\omega\phi$, the energy E is not 2π-periodic in ϕ. Therefore, its derivative on the boundary of the domain in ϕ is not well-defined. Consequently, it is difficult to analyze the global behavior of (9)–(11) using only the energy function (18).

IV. DEMARCATION OF DIFFERENT QUALITATIVE DYNAMICS IN THE (α, ω) PLANE

In Sec. III, we computed Lyapunov exponents of the dynamical system (9)–(11) and observed that they depend on the values of α and ω. In this section, we examine the dependence of the qualitative dynamics of (9)–(11) on the parameters α and ω.

We simulate 50 trajectories of the dynamical system (9)–(11) with initial conditions that we choose uniformly at random in $[-\pi,\pi)^3$. We set the mass of each oscillator to $m = 1$. We consider $\phi \in [-\pi,\pi)$ so that the oscillator phases satisfy 2π-periodicity, and we choose the domains of γ and k for simplicity. By varying the learning enhancement factor α and the intrinsic-frequency difference ω, we obtain three regions (which we label by Ω_1, Ω_2, and Ω_3) in the (α,ω) plane in which the trajectories exhibit qualitatively different dynamics.

In the region Ω_1, the dynamical system (9)–(11) does not have any equilibrium points. Our simulations suggest that all trajectories converge to a periodic solution. See Fig. 4 for an illustration. From Eq. (12), we infer that this region occurs when $0 < \alpha < 2\omega$. However, we have not proven rigorously that all trajectories converge to a single periodic solution, and we also have not proven whether or not this periodic solution is a limit cycle. To gain insight into this periodic solution, we use an approximation. In Ref. 38, Menck *et al.* approximated solutions near a limit cycle of a second-order power-grid model by assuming that oscillator phases rotate at

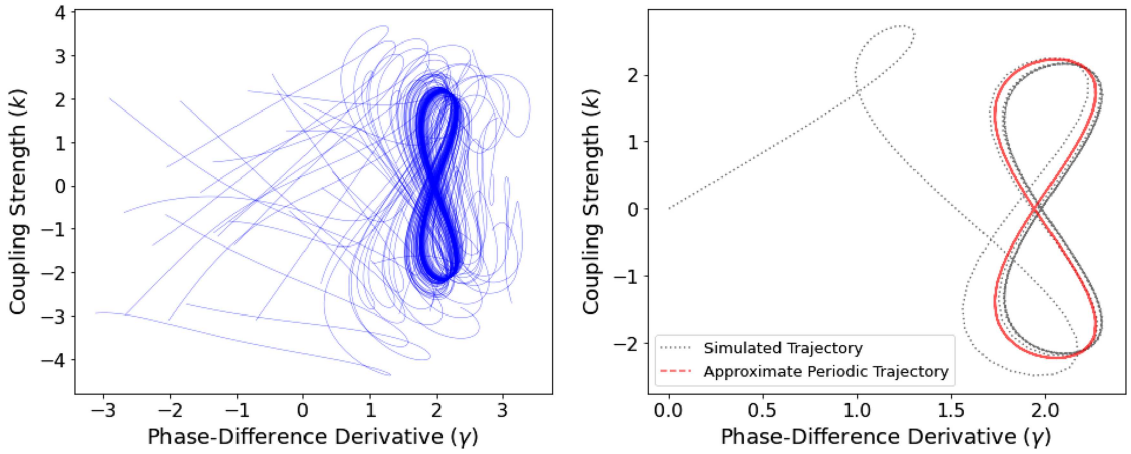

FIG. 4. We examine the projection onto the (γ,k) plane of simulated trajectories in the region Ω_1 for the two-oscillator system (9)–(11) with parameters $m = 1$, $\omega = 3$, and $\alpha = 5$. (Left) We simulate 50 trajectories with initial values that we choose uniformly at random in $[-\pi,\pi)^3$. (Right) We approximate the periodic trajectory that we observe in the region Ω_1.

a constant frequency. Inspired by this idea, we suppose that there exists $\zeta > 0$ (which we will determine later) such that $\phi(t) \approx \zeta t + \phi(0)$ and $\frac{d\phi}{dt} \approx \zeta$. We aim to parameterize $\gamma(t)$ and $k(t)$ by $\phi(t)$. Observe that Eq. (11) includes the term $\cos\phi$. Therefore, we posit an approximation of $k(t)$ of the form $k(t) \approx a\cos\phi(t) + b\sin\phi(t)$ for some constants a and b. Using the approximation $\frac{d\phi}{dt} \approx \zeta$ yields $\frac{dk}{dt} \approx (-a\sin\phi + b\cos\phi)\zeta$. Inserting the approximations of $k(t)$ and $\frac{dk}{dt}$ into Eq. (11) gives

$$(-a\sin\phi + b\cos\phi)\zeta + (a\cos\phi + b\sin\phi) \approx \alpha\cos\phi.$$

We now equate the coefficients of $\cos\phi$ and $\sin\phi$ to obtain $-a\zeta + b = 0$ and $b\zeta + a = \alpha$, and we then solve these two equations to obtain $a = \frac{\alpha}{\zeta^2+1}$ and $b = \frac{\alpha\zeta}{\zeta^2+1}$.

From Eq. (10) with $m = 1$, we have $\frac{d\gamma}{dt} + \gamma = \omega - k\sin\phi$. Similarly to our calculation above, we observe that Eq. (10) includes the term $k\sin\phi$. Recall from Eq. (9) that $\frac{d\phi}{dt} = \gamma$, so we posit an approximation of $\gamma(t)$ of the form $\gamma(t) \approx \zeta + c\cos 2\phi + d\sin 2\phi$ for some constants c and d. Inserting the approximations of $k(t)$ and $\gamma(t)$ into Eq. (10) with $m = 1$ yields

$$\begin{aligned}
&\zeta + (-2c\zeta + d)\sin 2\phi + (2d\zeta + c)\cos 2\phi \\
&\quad\approx \omega - \left(\frac{\alpha}{\zeta^2+1}\cos\phi + \frac{\alpha\zeta}{\zeta^2+1}\sin\phi\right)\sin\phi \\
&\quad\approx \omega - \frac{\alpha}{2(\zeta^2+1)}\sin 2\phi - \frac{\alpha\zeta}{\zeta^2+1}\left(\frac{1-\cos 2\phi}{2}\right) \\
&\quad\approx \omega - \frac{\alpha\zeta}{2(\zeta^2+1)} - \frac{\alpha}{2(\zeta^2+1)}\sin 2\phi + \frac{\alpha\zeta}{2(\zeta^2+1)}\cos 2\phi.
\end{aligned}$$

Equating the coefficients of $\cos 2\phi$ and $\sin 2\phi$ gives $\zeta = \omega - \frac{\alpha\zeta}{2(\zeta^2+1)}$, $-2c\zeta + d = -\frac{\alpha}{2(\zeta^2+1)}$, and $2d\zeta + c = \frac{\alpha\zeta}{2(\zeta^2+1)}$. Therefore, $c = \frac{3\zeta\alpha}{2(\zeta^2+1)(4\zeta^2+1)}$ and $d = \frac{(2\zeta^2-1)\alpha}{2(\zeta^2+1)(4\zeta^2+1)}$, where ζ is real and satisfies the equation $2\zeta^3 - 2\omega\zeta^2 + (\alpha+2)\zeta - 2\omega = 0$.

In summary, our approximation of the periodic solution satisfies

$$\begin{aligned}
\phi(t) &\approx \zeta t + \phi(0), \\
\gamma(t) &\approx \zeta + \frac{3\zeta\alpha}{2(\zeta^2+1)(4\zeta^2+1)}\cos 2\phi(t) \\
&\quad + \frac{(2\zeta^2-1)\alpha}{2(\zeta^2+1)(4\zeta^2+1)}\sin 2\phi(t), \\
k(t) &\approx \frac{\alpha}{\zeta^2+1}\cos\phi(t) + \frac{\alpha\zeta}{\zeta^2+1}\sin\phi(t),
\end{aligned}$$

where ζ is real and satisfies the equation $2x^3 - 2\omega x^2 + (\alpha+2)x - 2\omega = 0$. We have checked numerically that this polynomial equation always has a single real solution, so ζ is unique. As we can see in the right panel of Fig. 4, our approximate periodic solution is reasonably accurate. We have checked numerically that the phase difference ϕ increases approximately linearly with time. Therefore, our assumptions approximately hold in practice.

In the region Ω_2, the dynamical system (9)–(11) has four equilibrium points for $(\phi, \gamma, k) \in [-\pi, \pi) \times \mathbb{R} \times \mathbb{R}$. They are

$$\begin{aligned}
P_1 &= \left(\frac{1}{2}\arcsin\left(\frac{2\omega}{\alpha}\right), 0, \alpha\cos\left(\frac{1}{2}\arcsin\left(\frac{2\omega}{\alpha}\right)\right)\right), \\
P_2 &= \left(\frac{\pi}{2} - \frac{1}{2}\arcsin\left(\frac{2\omega}{\alpha}\right), 0, \alpha\sin\left(\frac{1}{2}\arcsin\left(\frac{2\omega}{\alpha}\right)\right)\right), \\
P_3 &= \left(-\pi + \frac{1}{2}\arcsin\left(\frac{2\omega}{\alpha}\right), 0, -\alpha\cos\left(\frac{1}{2}\arcsin\left(\frac{2\omega}{\alpha}\right)\right)\right), \\
P_4 &= \left(-\frac{\pi}{2} - \frac{1}{2}\arcsin\left(\frac{2\omega}{\alpha}\right), 0, -\alpha\sin\left(\frac{1}{2}\arcsin\left(\frac{2\omega}{\alpha}\right)\right)\right).
\end{aligned}$$

In this region, there exists a heteroclinic orbit that connects the equilibrium points P_2 and P_4. This situation is rather different from the periodic dynamics that we observed in the region Ω_1. As one can

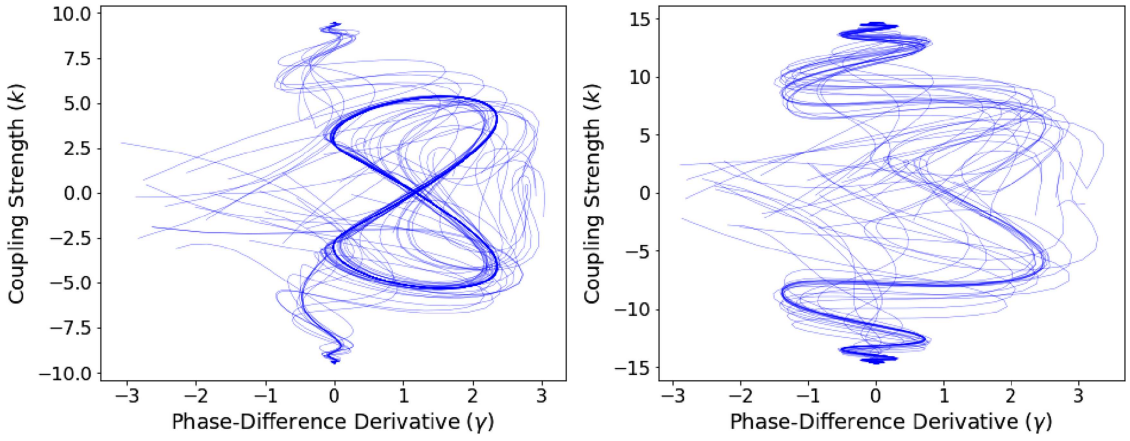

FIG. 5. (Left) Projection onto the (γ, k) plane of simulated trajectories in the region Ω_2 for the two-oscillator system (9)–(11) with parameters $m = 1$, $\omega = 3$, and $\alpha = 10$. (Right) Projection onto the (γ, k) plane of simulated trajectories in the region Ω_3 for the dynamical system (9)–(11) with parameters $m = 1$, $\omega = 3$, and $\alpha = 15$.

see in our simulations in the left panel of Fig. 5, some trajectories converge to the equilibrium points but others converge to this heteroclinic orbit. By contrast, in the region Ω_3 (see the right panel of Fig. 5), we observe that all simulated trajectories converge to the equilibrium points and that there is not a heteroclinic orbit. When we fix ω and gradually increase α, the behaviors of the trajectories progress from the dynamics that we observe in the region Ω_1 to those that we observe in Ω_2 and finally to those in Ω_3. Therefore, we conjecture that for each fixed ω, there exists a value α_ω of α such that Ω_2 corresponds to the region with $2\omega \leq \alpha \leq \alpha_\omega$ and Ω_3 corresponds to the region with $\alpha_\omega < \alpha$.

We seek to approximate the three regions Ω_1, Ω_2, and Ω_3 in the (α, ω) plane to gain insight into α_ω. We do this with numerical simulations and use a coarse approach to check whether or not there exists a heteroclinic orbit that connects P_2 and P_4. We assume that $(\alpha, \omega) \in [0, 36] \times [0, 2\pi)$, and we then divide this rectangular domain into a grid with 150×150 points and consider the parameter values (α, ω) at each grid point. For each value of (α, ω), because the phase ϕ has period 2π, we consider the Poincaré section $\mathcal{P} = \{(\phi, \gamma, k) | \phi = 0\}$. We pick 20 uniformly random initial values in the rectangle $R = \{0\} \times [-\pi, \pi) \times [-\pi, \pi)$ in $\mathcal{P}$. If the dynamical system (9)–(11) has a heteroclinic orbit, then a small perturbation of that orbit yields a trajectory that has multiple intersections with $\mathcal{P}$.

For each initial condition, we integrate for 1000 time steps and we classify the resulting region based on the mean number of times that a trajectory intersects $\mathcal{P}$. In practice, we find that if a trajectory converges to an equilibrium point, then it only intersects $\mathcal{P}$ once or twice. Our approach yields a rough estimate of the regions Ω_1, Ω_2, and Ω_3 (see Fig. 6); it does not precisely determine the boundaries between these regions.

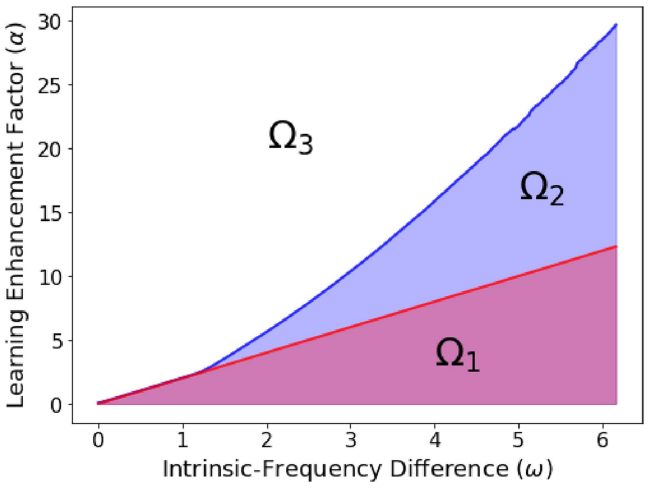

FIG. 6. Approximate regions in the (α, ω) plane for which the two-oscillator system (9)–(11) has different qualitative dynamics. The region Ω_1 consists of the parameter values (α, ω) for which the dynamical system (9)–(11) does not have any equilibrium points. The regions Ω_2 and Ω_3, respectively, consist of the parameter values (α, ω) for which the dynamical system (9)–(11) has equilibrium points with heteroclinic orbits and without heteroclinic orbits.

V. A PRELIMINARY INVESTIGATION OF OUR HEBBIAN KURAMOTO MODEL WITH MANY OSCILLATORS

In Sec. IV, we observed that the qualitative dynamics of the trajectories of the 3D dynamical system (9)–(11) depend on the oscillators' intrinsic-frequency difference ω and the learning enhancement factor α. We now use these insights to motivate a preliminary investigation of our Hebbian Kuramoto model [see Eqs. (1) and (2)] in high-dimensional situations (i.e., with many oscillators).

We consider a specific setup for the intrinsic oscillator frequencies ω_i (with $i \in \{1, \ldots, N\}$) by sampling them randomly from a Gaussian distribution with mean 0 and variance $\mathcal{N}(0, \sigma^2)$ for different values of σ. We expect that the variance σ^2 in our high-dimensional Hebbian Kuramoto model plays a role that is analogous to the intrinsic-frequency difference ω in the 3D system (9)–(11).

In our study of the low-dimensional transverse system (9)–(11), we suppose that the mass of each oscillator is $m = 1$. In a high-dimensional Hebbian Kuramoto model [see Eqs. (1) and (2)], we expect that the inertia terms play a significant role in the synchronization of the oscillators. In our numerical computations, we consider a coupled system of $N = 50$ oscillators. By increasing the value of inertia, Olmi *et al.*[39] observed that their Kuramoto model with inertia (without any adaptation) has a partially synchronized state. In addition to a cluster of phase-locked oscillators with $\frac{d\phi_i}{dt} \approx 0$, they also observed clusters of phase-locked oscillators with finite mean velocities $\frac{d\phi_i}{dt} \not\approx 0$. Such additional clusters are called "drifting coherent clusters" of oscillators. Adaptive Kuramoto models without inertia also develop clusters of phase-locked oscillators.[20,32] Both with and without inertia, the formation of clusters of oscillators can depend on the adaptation rule.

Niyogi and English[26] observed for complete networks that the Kuramoto model (without inertia) with the adaptation rule (2) eventually develops two stable synchronized clusters in anti-phase when the learning rate is larger than a critical value. To account for the possibility of two phase-locked clusters of oscillators, we examine the order parameter

$$r_2(t) = \left| \frac{1}{N} \sum_{j=1}^{N} e^{2i\phi_j(t)} \right|. \tag{19}$$

We perform numerical simulations to investigate how $r_2(t)$ changes with time. We consider two systems of $N = 50$ coupled oscillators. Suppose that each oscillator i has the same mass $m_i = m$. We consider examples with light masses ($m = 1$) and heavy masses ($m = 100$). Each system consists of $\frac{50(51)}{2} = 1275$ coupled differential equations. We set the initial phases of the oscillators to be evenly spaced in $[0, 2\pi)$, the initial phase derivatives to $\phi_i'(0) = 0$, and the initial coupling strengths to $K_{ij} = 1$. We investigate the effects of α and σ^2 on the order parameter $r_2(t)$ by fixing one of these two parameters and varying the other. We show our results in Figs. 7 and 8.

For both light masses and heavy masses, we observe that the order parameter $r_2(t) \to 1$ when $\sigma^2 \ll \alpha$, suggesting that almost all oscillators are either in a single fully synchronized cluster or that there are two phase-locked clusters. In both cases, we also observe that the oscillators are incoherent when $\sigma^2 \gg \alpha$. When the oscillators are not entirely in either one or two phase-locked clusters, we

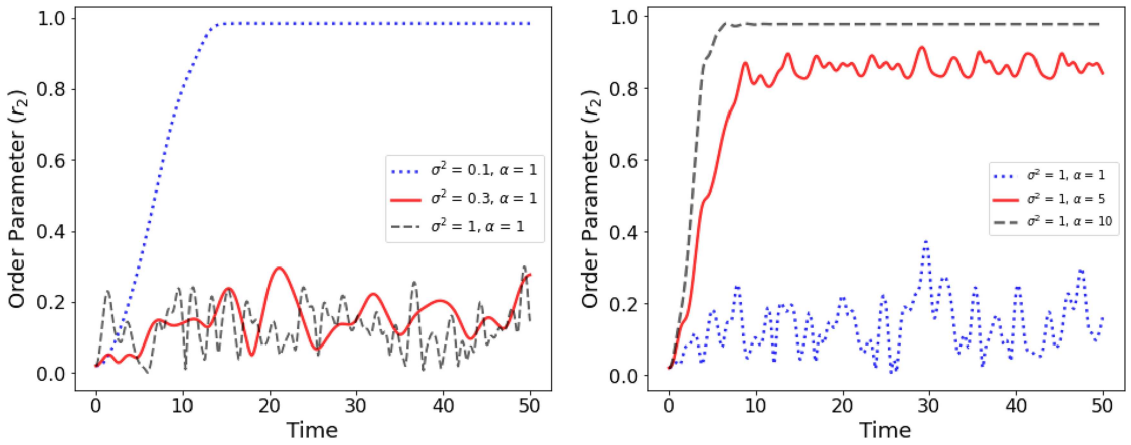

FIG. 7. The order parameter $r_2(t)$ for our Hebbian Kuramoto model [see Eqs. (1) and (2)] with $N = 50$ oscillators of mass $m = 1$. (Left) We fix the learning enhancement factor to $\alpha = 1$ and consider variances of $\sigma^2 = 0.1$, $\sigma^2 = 0.3$, and $\sigma^2 = 1$. (Right) We fix the variance to $\sigma^2 = 1$ and consider learning enhancement factors of $\alpha = 1$, $\alpha = 5$, and $\alpha = 10$. For each simulation, we draw a new set of natural oscillator frequencies from the specified distribution. Therefore, the order parameters for $\sigma^2 = 1$ and $\alpha = 1$ are different in the two panels.

observe oscillations in the order parameter, with a more pronounced amplitude for heavy masses than for light masses. When $r_2(t)$ oscillates, we observe multiple drifting coherent clusters of oscillators in addition to the two large phase-locked clusters. We observe more drifting coherent clusters for heavy masses than for light masses.

Heuristically, when adaptivity dominates inertia (specifically, when the mass m is small and $\alpha \gg \sigma^2$), the oscillators tends to form one or two phase-locked clusters because of Hebbian learning. However, when the mass m is large, inertia delays the formation of such phase-locked clusters. Consequently, the interplay between adaptivity and inertia yields small drifting coherent clusters that resemble those that Olmi *et al.*[39] observed in a nonadaptive Kuramoto model with inertia. We thus observe oscillations in the order parameter $r_2(t)$.

The qualitative dynamics of our high-dimensional Hebbian Kuramoto model [see Eqs. (1) and (2)], which we examined with 50 oscillators, resembles the dynamics that we observed in the transverse two-oscillator system (9)–(11). In the 50-oscillator system, for fixed values of σ^2 and ω, as we increase the value of α, the incoherent oscillators experience progressively more phase-locking until eventually most of the oscillators are in one or two phase-locked clusters. In the transverse two-oscillator system, for fixed σ^2 and ω, as we increase the value of α, progressively more trajectories converge to the equilibrium points P_1 and P_3.

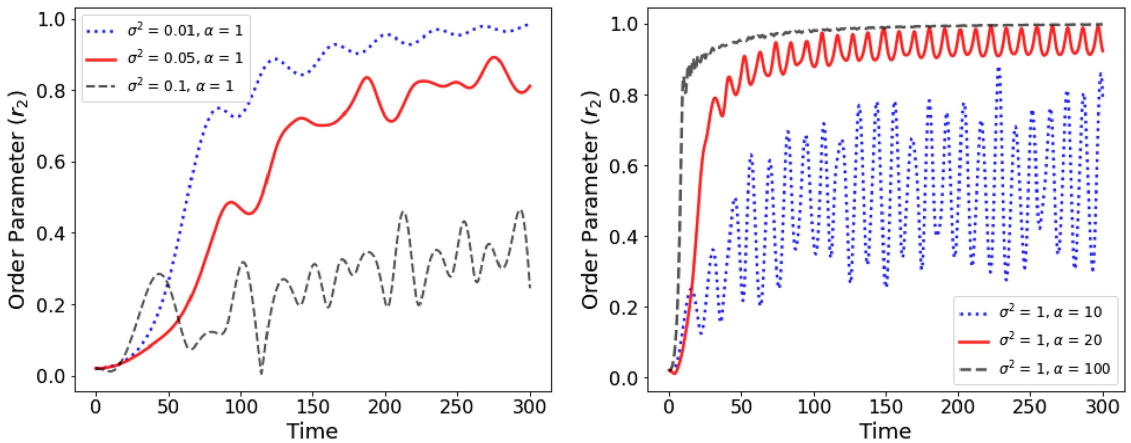

FIG. 8. The order parameter $r_2(t)$ for our Hebbian Kuramoto model [see Eqs. (1) and (2)] with $N = 50$ oscillators of mass $m = 100$. (Left) We the fix the learning enhancement factor to $\alpha = 1$ and consider variances of $\sigma^2 = 0.01$, $\sigma^2 = 0.05$, and $\sigma^2 = 0.1$. (Right) We fix the variance to $\sigma^2 = 1$ and consider learning enhancement factors of $\alpha = 10$, $\alpha = 20$, and $\alpha = 100$.

VI. CONCLUSIONS

We studied an adaptive Kuramoto model with inertia in which the coupling strengths between phase oscillators depend on a Hebbian learning rule. We mostly examined a system with $N = 2$ coupled oscillators. This yields a 5D dynamical system, which decouples into a 3D transverse system and a 2D longitudinal system. Our analysis and numerical simulations of the transverse system suggest that it has three different types of qualitative behavior, which depends on the learning enhancement factor α and the intrinsic-frequency difference ω between the two oscillators.

Our insights from studying a two-oscillator Hebbian Kuramoto model suggest choices of parameter values in associated high-dimensional models. We conducted numerical simulations of a 50-oscillator system in which we drew the intrinsic frequencies of the oscillators from a Gaussian distribution with 0 mean. We observed that the variance of the oscillators' intrinsic frequencies in the high-dimensional system plays a role that is similar to the intrinsic-frequency difference ω in the low-dimensional system. As we increased the learning enhancement factor α, we observed that the high-dimensional system of coupled oscillators transitions from an incoherent state to a partially phase-locked state with drifting coherent clusters and finally to a state with at most two almost fully phase-locked clusters.

The dependence of our Hebbian Kuramoto model's behavior on the learning enhancement factor and intrinsic oscillator frequencies has a neuroscientific analog. In neuroscience, long-term potentiation (LTP) synapses and long-term depression (LDP) synapses refer, respectively, to types of synapses in which presynaptic neurons repeatedly promote and inhibit postsynaptic neurons.[40] In a model of a neuronal system as a set of coupled oscillators, LTP describes a situation with all oscillators in phase and LDP describes a situation with oscillators split into two groups that are in anti-phase with respect to each other.[26] Based on (1) our observation that the trajectories in our transverse two-oscillator system converge either to a periodic orbit or to one of two equilibrium points and (2) the dynamics of the order parameter $r_2(t)$, which captures the synchrony of two phase-locked clusters of oscillators, our Kuramoto model with inertia and Hebbian learning suggests that the behaviors of the oscillators are simplistic analogs of the behaviors of LTP and LDP synapses in neuronal networks.

A natural extension of our work is a systematic analysis of how different values of inertia affect the transition to phase-locked groups of oscillators for all values of the other system parameters. To better understand the interaction between phase-locked oscillator clusters and drifting oscillators, it is desirable to conduct a thorough investigation of the formation of drifting coherent clusters. In the transverse two-oscillator system (9)–(11), it seems worthwhile to obtain an analytical description of how the boundary between the regions Ω_2 and Ω_3 changes with changes in inertia. We hope that a better understanding of the demarcation between Ω_2 and Ω_3 can provide further insight into the qualitative dynamics in different regions of parameter space of our N-oscillator (i.e., high-dimensional) Hebbian Kuramoto model [see Eqs. (1) and (2)].

ACKNOWLEDGMENTS

We thank Predrag Cvitanović, Christian Kuehn, and two anonymous referees for helpful comments.

AUTHOR DECLARATIONS

Conflict of Interest

The authors have no conflicts to disclose.

Author Contributions

Tachin Ruangkriengsin: Conceptualization (equal); Formal analysis (lead); Investigation (lead); Methodology (lead); Software (lead); Visualization (lead); Writing – original draft (lead); Writing – review & editing (supporting). **Mason A. Porter:** Conceptualization (equal); Methodology (supporting); Project administration (lead); Supervision (lead); Writing – review & editing (lead).

DATA AVAILABILITY

All of the data in this article are outputs of numerical computations.

APPENDIX: PROOF OF PROPOSITION 1

We first recall the statement of Proposition 1.

Proposition 1. *Consider the dynamical system (9)–(11) with $\alpha > 2\omega$. Let $u := \alpha + \sqrt{\alpha^2 - 4\omega^2}$ and $v := \alpha - \sqrt{\alpha^2 - 4\omega^2}$. The following statements hold:*

1. *Let Γ_1 be the region in the (u, v) plane with $0 \le v \le u \le \frac{2(m^2-m+1)}{3m}$ that is bounded by the curves*

$$v = u - \frac{\left(m+1+\sqrt{4(m+1)^2-6m(u+2)}\right)\left(\sqrt{4(m+1)^2-6m(u+2)}-2(m+1)\right)^2}{54m^2},$$

$$v = u - \frac{\left(m+1-\sqrt{4(m+1)^2-6m(u+2)}\right)\left(\sqrt{4(m+1)^2-6m(u+2)}+2(m+1)\right)^2}{54m^2}.$$

If $(u, v) \notin \Gamma_1$, then the Jacobian matrix at the equilibria P_1 and P_3 has a negative real eigenvalue and two complex-conjugate eigenvalues with a negative real part. Otherwise, the Jacobian matrix at the equilibria P_1 and P_3 has three negative real eigenvalues.

2. *Let Γ_2 be the region in the (u,v) plane with $0 \le v \le u$ and $v \le \frac{2(m^2-m+1)}{3m}$ that is bounded by the curves*

$$u = v - \frac{\left(m+1+\sqrt{4(m+1)^2-6m(v+2)}\right)\left(\sqrt{4(m+1)^2-6m(v+2)}-2(m+1)\right)^2}{54m^2},$$

$$u = v - \frac{\left(m+1-\sqrt{4(m+1)^2-6m(v+2)}\right)\left(\sqrt{4(m+1)^2-6m(v+2)}+2(m+1)\right)^2}{54m^2}.$$

If $(u,v) \notin \Gamma_2$, the Jacobian matrix at the equilibria P_2 and P_4 has a positive real eigenvalue and two complex-conjugate eigenvalues with a negative real part. Otherwise, the Jacobian matrix at the equilibria P_2 and P_4 has one positive real eigenvalue and two negative real eigenvalues.

Proof. We first consider the region Γ_1, which is the region in the (α,ω) plane for which the equilibria P_1 and P_3 have three negative real eigenvalues. From Eq. (15), we need to consider the values of α and ω for which the polynomial

$$\begin{aligned} f(x) &:= 2x(x+1)(mx+1) + \left(\alpha+\sqrt{\alpha^2-4\omega^2}\right)(x+1) \\ &\quad - \left(\alpha-\sqrt{\alpha^2-4\omega^2}\right) \\ &= 2mx^3 + 2(m+1)x^2 + (u+2)x + u - v \end{aligned}$$

has three real roots. When $\alpha > 2\omega \ge 0$, we see that u and v are real, with $u \ge v \ge 0$. Therefore, because $f(x)$ is a degree-3 polynomial with real coefficients, it must have either three real roots or one real root and two complex-conjugate roots. The boundary of the region Γ_1 occurs when $f(x)$ has a double root $\tilde{x}$. Therefore, we also consider

$$f'(x) = 6mx^2 + 4(m+1)x + u + 2.$$

The root $\tilde{x}$ satisfies both $f(x) = 0$ and $f'(x) = 0$, so it satisfies

$$\begin{aligned} Q(x) &:= 3f(x) - xf'(x) \\ &= 2(m+1)x^2 + 2(u+2)x + 3(u-v) = 0. \end{aligned}$$

We obtain $\tilde{x}$ by solving

$$\begin{aligned} 0 &= (m+1)f'(\tilde{x}) - 3mQ(\tilde{x}) \\ &= (4(m+1)^2 - 6(u+2)m)\tilde{x} - (9m(u-v) - (u+2)(m+1)) \end{aligned}$$

to yield

$$\tilde{x} = \frac{9m(u-v) - (u+2)(m+1)}{4(m+1)^2 - 6(u+2)m}.$$

The value $\tilde{x}$ must also satisfy $f'(x) = 0$, so

$$\tilde{x} = \frac{9m(u-v) - \left(\frac{4(m+1)^2-s}{6m}\right)(m+1)}{s} = \frac{-(m+1) \pm 2\sqrt{s}}{12m}, \tag{A1}$$

where $s := 4(m+1)^2 - 6(u+2)m$. Rearranging Eq. (A1) yields

$$\begin{aligned} u - v &= \frac{\pm s\sqrt{s} - 3s(m+1) + 4(m+1)^3}{54m^2} \\ &= \frac{\left(\pm\sqrt{s}+m+1\right)\left(\sqrt{s}\mp 2(m+1)\right)^2}{54m^2}. \end{aligned} \tag{A2}$$

The choice of signs in Eq. (A2) (where the upper and lower sign choices correspond) gives the two boundary curves in the proposition. For $\tilde{x}$ to be real, we require that $s \ge 0$, which implies that $u \ge \frac{2(m^2-m+1)}{3m}$. We obtain Eq. (16) by swapping the variables u and v in Eq. (15). We then obtain the boundary curves of the region Γ_2 using the same calculation with u and v swapped.

We now determine the signs of the eigenvalues of the Jacobian matrix at the equilibrium points P_1 and P_3. Observe that $f(0) = 2\sqrt{\alpha^2-4\omega^2}$ and $f(-1) = -\left(\alpha-\sqrt{\alpha^2-4\omega^2}\right)$. Consequently, by the Intermediate Value Theorem, there exists at least one negative real root of $f(x)$ in the interval $[-1,0)$. By Vieta's Theorem, the sum of all of the roots is $-1-\frac{1}{m} < -1$ and the product of these roots is $\frac{v-u}{2m} < 0$. Therefore, the sum of the other two roots must be negative and the product of these other two roots must be positive. This implies that these other two roots have negative real parts. Therefore, the eigenvalues of the Jacobian matrix at the equilibria P_1 and P_3 all have negative real parts.

We also determine the signs of the eigenvalues of the Jacobian matrix at the equilibrium points P_2 and P_4. Let

$$\begin{aligned} g(x) &:= -2x(x+1)(mx+1) - \left(\alpha-\sqrt{\alpha^2-4\omega^2}\right)(x+1) \\ &\quad + \left(\alpha+\sqrt{\alpha^2-4\omega^2}\right) \end{aligned}$$

be the left-hand side of Eq. (16). Observe that $g(0) = 2\sqrt{\alpha^2-4\omega^2} > 0$ and that $g\left(\frac{2\sqrt{\alpha^2-4\omega^2}}{\alpha-\sqrt{\alpha^2-4\omega^2}}\right) = -\frac{4\sqrt{\alpha^2-4\omega^2}\left(\alpha+\sqrt{\alpha^2-4\omega^2}\right)}{\left(\alpha-\sqrt{\alpha^2-4\omega^2}\right)^2} < 0$. By the Intermediate Value Theorem, there exists at least one positive real root of $g(x)$ in the interval $\left(0, \frac{2\sqrt{\alpha^2-4\omega^2}}{\alpha-\sqrt{\alpha^2-4\omega^2}}\right)$. By Vieta's Theorem, the sum of all of the roots is $-1-\frac{1}{m} < 0$ and the product of the roots is $\frac{u-v}{2m} > 0$. Therefore, the sum of the other two roots must be negative and the product of these other two roots must be positive. This implies that these other two roots have negative real parts. □

REFERENCES

[1] A. Pikovsky and M. Rosenblum, "Synchronization," Scholarpedia **2**, 1459 (2007).
[2] P. Mateos-Aparicio and A. Rodríguez-Moreno, "The impact of studying brain plasticity," Front. Cell. Neurosci. **13**, 402 (2019).
[3] G. B. Ermentrout, "An adaptive model for synchrony in the firefly *Pteroptyx malaccae*," J. Math. Biol. **29**, 571–585 (1991).

[4]S. H. Strogatz, "From Kuramoto to Crawford: Exploring the onset of synchronization in populations of coupled oscillators," Physica D **143**, 1 (2000).
[5]R. E. Mirollo and S. H. Strogatz, "Synchronization of pulse-coupled biological oscillators," SIAM J. Appl. Math. **50**, 1645 (1990).
[6]S. H. Strogatz, D. M. Abrams, A. McRobie, B. Eckhardt, and E. Ott, "Crowd synchrony on the Millennium Bridge," Nature **438**, 43 (2005).
[7]I. Belykh, M. Bocian, A. R. Champneys, K. Daley, R. Jeter, J. H. G. Macdonald, and A. McRobie, "Emergence of the London Millennium Bridge instability without synchronisation," Nat. Commun. **12**, 7223 (2021).
[8]D. C. Michaels, E. P. Matyas, and J. Jalife, "Mechanisms of sinoatrial pacemaker synchronization: A new hypothesis," Circ. Res. **61**, 704 (1987).
[9]K. Ota, I. Aihara, and T. Aoyagi, "Interaction mechanisms quantified from dynamical features of frog choruses," R. Soc. Open Sci. **7**, 191693 (2020).
[10]Y. Kuramoto, *Chemical Oscillations, Waves, and Turbulence* (Springer-Verlag, Heidelberg, Germany, 1984).
[11]F. Rodrigues, T. K. D. Peron, P. Ji, and J. Kurths, "The Kuramoto model in complex networks," Phys. Rep. **610**, 1 (2016).
[12]B. R. Trees, V. Saranathan, and D. Stroud, "Synchronization in disordered Josephson junction arrays: Small-world connections and the Kuramoto model," Phys. Rev. E **71**, 016215 (2005).
[13]M. Rohden, A. Sorge, M. Timme, and D. Witthaut, "Self-organized synchronization in decentralized power grids," Phys. Rev. Lett. **109**, 064101 (2012).
[14]H.-A. Tanaka, A. J. Lichtenberg, and S. Oishi, "Self-synchronization of coupled oscillators with hysteretic responses," Physica D **100**, 279 (1997).
[15]D. O. Hebb, *The Organization of Behavior* (John Wiley & Sons, Inc., Hoboken, NJ, USA, 1964).
[16]D. Ghosh, M. Frasca, A. Rizzo, S. Majhi, S. Rakshit, K. Alfaro-Bittner, and S. Boccaletti, "The synchronized dynamics of time-varying networks," Phys. Rep. **949**, 1 (2022).
[17]R. Berner, T. Gross, C. Kuehn, J. Kurths, and S. Yanchuk, "Adaptive dynamical networks," Phys. Rep. **1031**, 1–59 (2023).
[18]J. Sawicki *et al.*, "Perspectives on adaptive dynamical systems," Chaos **33**, 071501 (2023).
[19]B. Jüttner and E. A. Martens, "Complex dynamics in adaptive phase oscillator networks," Chaos **33**, 053106 (2023).
[20]R. Berner, E. Schöll, and S. Yanchuk, "Multiclusters in networks of adaptively coupled phase oscillators," SIAM J. Appl. Dyn. Syst. **18**, 2227 (2019).
[21]J. Fialkowski, S. Yanchuk, I. M. Sokolov, E. Schöll, G. A. Gottwald, and R. Berner, "Heterogeneous nucleation in finite-size adaptive dynamical networks," Phys. Rev. Lett. **130**, 067402 (2023).
[22]R. Berner, J. Sawicki, and E. Schöll, "Birth and stabilization of phase clusters by multiplexing of adaptive networks," Phys. Rev. Lett. **124**, 088301 (2020).
[23]A. D. Kachhvah and S. Jalan, "First-order route to antiphase clustering in adaptive simplicial complexes," Phys. Rev. E **105**, L062203 (2022).
[24]M. A. Gkogkas, C. Kuehn, and C. Xu, "Mean field limits of co-evolutionary heterogeneous networks," arXiv:2202.01742 (2022).
[25]M. A. Gkogkas, C. Kuehn, and C. Xu, "Continuum limits for adaptive network dynamics," Commun. Math. Sci. **21**, 83–106 (2023).
[26]R. K. Niyogi and L. Q. English, "Learning-rate-dependent clustering and self-development in a network of coupled phase oscillators," Phys. Rev. E **80**, 066213 (2009).
[27]L. Timms and L. Q. English, "Synchronization in phase-coupled Kuramoto oscillator networks with axonal delay and synaptic plasticity," Phys. Rev. E **89**, 032906 (2014).
[28]P. Seliger, S. C. Young, and L. S. Tsimring, "Plasticity and learning in a network of coupled phase oscillators," Phys. Rev. E **65**, 041906 (2002).
[29]Q. Ren and J. Zhao, "Adaptive coupling and enhanced synchronization in coupled phase oscillators," Phys. Rev. E **76**, 016207 (2007).
[30]S.-Y. Ha, S. E. Noh, and J. Park, "Synchronization of Kuramoto oscillators with adaptive couplings," SIAM J. Appl. Dyn. Syst. **15**, 162–194 (2016).
[31]T. Aoki and T. Aoyagi, "Self-organized network of phase oscillators coupled by activity-dependent interactions," Phys. Rev. E **84**, 066109 (2011).
[32]R. Berner, S. Yanchuk, and E. Schöll, "What adaptive neuronal networks teach us about power grids," Phys. Rev. E **103**, 042315 (2021).
[33]A. S. Pikovsky and P. Grassberger, "Symmetry breaking bifurcation for coupled chaotic attractors," J. Phys. A: Math. Gen. **24**, 4587 (2007).
[34]S. Olmi, "Chimera states in coupled Kuramoto oscillators with inertia," Chaos **25**, 123125 (2015).
[35]M. Sandri, "Numerical calculation of Lyapunov exponents," Math. J. **6**, 78 (1996).
[36]G. Benettin, L. Galgani, A. Giorgilli, and J.-M. Strelcyn, "Lyapunov characteristic exponents for smooth dynamical systems and for Hamiltonian systems; a method for computing all of them. Part 1: Theory," Meccanica **15**, 9 (1980).
[37]M. Klein and G. Baier, "Hierarchies of dynamical systems," in *A Chaotic Hierarchy*, edited by M. Klein and G. Baier (World Scientific, Singapore, 1991), pp. 1–23.
[38]P. J. Menck, J. Heitzig, J. Kurths, and H. J. Schellnhuber, "How dead ends undermine power grid stability," Nat. Commun. **5**, 3969 (2014).
[39]S. Olmi, A. Navas, S. Boccaletti, and A. Torcini, "Hysteretic transitions in the Kuramoto model with inertia," Phys. Rev. E **90**, 042905 (2014).
[40]T. V. P. Bliss and S. F. Cooke, "Long-term potentiation and long-term depression: A clinical perspective," Clinics **66**, 3 (2011).